IOP Publishing Journal of Physics: Condensed Matter
J. Phys.: Condens. Matter **32** (2020) 225705 (6pp) https://doi.org/10.1088/1361-648X/ab7576

High-throughput first-principles screening of layered magnetic double perovskites $Cs_4MSb_2X_{12}$ for spintronic applications

Dan Han[1,2,4], **Tao Zhang**[1,4] **and Shiyou Chen**[1,3]

[1] Key Laboratory of Polar Materials and Devices (Ministry of Education) and Department of Electronics, East China Normal University, Shanghai 200241, People's Republic of China
[2] Department of Chemistry, Ludwig-Maximilians-Universität, München D81377, Germany
[3] Collaborative Innovation Center of Extreme Optics, Shanxi University, Shanxi 030006, People's Republic of China

E-mail: chensy@ee.ecnu.edu.cn

Received 3 October 2019, revised 3 January 2020
Accepted for publication 12 February 2020
Published 5 March 2020

Abstract

Double perovskite halides have drawn great attention due to characteristics of non-toxicity, stability and broad elemental compositions compared to $CH_3NH_3PbI_3$. Among them, layered double perovskite halides have been proposed as promising photovoltaic materials. Noteworthily, layered materials have been extensively explored as spintronic materials. Can layered double perovskites act as spintronic material and thus extend the application from optoelectronics to spintronics? In this paper, we investigated a series of ⟨1 1 1⟩-oriented layered magnetic double perovskites by high-throughput first-principles calculations to find suitable spintronic candidates. Three thermodynamically stable layered double perovskites $Cs_4MnSb_2Cl_{12}$, $Cs_4CuSb_2Cl_{12}$ and $Cs_4ScSb_2Br_{12}$ are identified. The ground state structure of $Cs_4MnSb_2Cl_{12}$ has the *R-3m* symmetry and exhibits antiferromagnetic (AFM) ordering, while $Cs_4CuSb_2Cl_{12}$ favors the *C*2/*m* symmetry and shows AFM ordering, which are in line with the experimental observations. $Cs_4MnSb_2Cl_{12}$ and $Cs_4CuSb_2Cl_{12}$ are AFM semiconductors. Additionally, a new layered double perovskite $Cs_4ScSb_2Br_{12}$ is predicted for the first time, favoring the *C*2/*m* symmetry and showing metallicity and AFM ordering, which may be synthesized experimentally in the future.

Keywords: layered double perovskite, spintronics, high-throughput first-principles calculation

Supplementary material for this article is available online

(Some figures may appear in colour only in the online journal)

1. Introduction

Double perovskite halides $A_2M(I)M(III)X_6$ have been proposed as one kind of alternative to $CH_3NH_3PbI_3$ due to their supreme air-stability and non-toxic characters [1–6]. So far, the reported double perovskite halides have large band gaps and most of them are indirect [7, 8], which are not suitable for the application in single-junction solar cells [9] but could be employed in multi-junction solar cells. Interestingly, double perovskite halides have been introduced into spintronic field recently besides photovoltaic application.[10] Cai *et al* found double perovskite halides Cs_2GeMnX_6 (X = Cl, Br and I) are promising ferromagnetic (FM) spintronic materials with the excellent properties, i.e. structural stability, large spin splitting and high T_C, which extends the perovskite-based optoelectronics to perovskite-based spintronics [10].

Recently, layered double perovskite halides emerged as optoelectronic and photoelectrochemical materials [11–16]. A

[4] These authors contributed equally to this work.

new type of ⟨1 1 1⟩-oriented layered double perovskite halide $Cs_4CuSb_2Cl_{12}$ has been successfully synthesized, showing great potential as a photovoltaic material [13]. In addition, the photovoltaic applications of $Cs_{3+n}M(II)_nSb_2X_{9+3n}$ (M = Sn, Ge) have been studied [12]. Meanwhile, the optoelectronic properties of $Cs_4CuSb_2Cl_{12}$-like $Cs_4M^{2+}B_2^{3+}X_{12}^{VII}$ as p-type transparent conductors have been investigated [14]. We could see layered double perovskite halides have been mainly explored as optoelectronic and photoelectrochemical materials at present. However, it is noteworthy that layered materials such as Cr-based materials as well as the corresponding low-dimensional compounds can be spintronic materials [17–21]. Double perovskite halides Cs_2GeMnX_6 (X = Cl, Br and I) are promising spintronic materials with supreme properties. How about layered double perovskite halides? Can layered double perovskite halides containing transition metals be spintronics materials? It's still an open question considering that there are limited investigations of magnetic layered double perovskite.

In this work, via high-throughput first-principles calculations, we investigated a series of ⟨1 1 1⟩-oriented layered double perovskites $Cs_4MSb_2X_{12}$ (M: +2 transition metals, X: Cl, Br and I), and identified three thermodynamically stable layered double perovskites $Cs_4MnSb_2Cl_{12}$, $Cs_4CuSb_2Cl_{12}$ and $Cs_4ScSb_2Br_{12}$ as potential spintronic materials. The ground state structure of $Cs_4MnSb_2Cl_{12}$ has the *R*-3*m* symmetry and exhibits AFM ordering, while the $Cs_4CuSb_2Cl_{12}$ and $Cs_4ScSb_2Br_{12}$ favor the *C*2/*m* symmetry and show AFM ordering. We did not find thermodynamically stable $Cs_4MSb_2X_{12}$ showing FM ordering. Even so, our high-throughput calculation is valid for searching the thermodynamically stable ⟨1 1 1⟩ layered magnetic double perovskites considering that our calculated results are in line with the experimental observations, i.e. the ground state structures of $Cs_4MnSb_2Cl_{12}$ and $Cs_4CuSb_2Cl_{12}$ have *R*-3*m* and *C*2/*m* symmetry, respectively, and they both exhibit AFM behavior. In addition, a new layered double perovskite $Cs_4ScSb_2Br_{12}$ showing metallicity is predicted for the first time, and it may be synthesized experimentally in the future.

2. Methods

The first-principles calculations were carried out using spin-polarized density functional theory with exchange functional of Perdew–Burke–Ernzerhof (PBE) [22] within the generalized gradient approximation as implemented in the Vienna *ab initio* simulation package (VASP) [23, 24]. To describe the ion-electron interaction, the projected augmented wave potential was used [25]. A plane-wave cutoff of 520 eV was used for all calculations. Based on the experimental structures of $Cs_4CuSb_2Cl_{12}$ in *C*2/*m* phase [13] and $Cs_4MnSb_2Cl_{12}$ in *R*-3*m* phase [15], halogen and all possible transition mental elements showing divalent charged states were substituted into those structures to obtain $Cs_4MSb_2X_{12}$ (M: +2 transition metals; X: Cl, Br and I), as shown in figure 1. Considering possible effect of strongly correlated electrons, we performed GGA + *U* calculations [26] and used reported effective *U* values for transition metals [27–30]. All lattice vectors and atomic positions are fully relaxed until the force on each atom is smaller than 0.02 eV $Å^{-1}$.

For the Brillouin zone integration, 3 × 3 × 2 and 4 × 4 × 1 Γ-centered *k*-meshes were used for FM configurations in *C*2/*m* phase and *R*-3*m* phase, respectively. Taking $Cs_4CuSb_2Cl_{12}$ as an example, the lattice constants of its FM configurations in *C*2/*m* phase are $a = b = 7.734$ Å, and $c = 13.445$ Å and the lattice constants in *R*-3*m* phase are $a = b = 7.548$ Å, and $c = 36.682$ Å. Using 3 × 3 × 2 and 4 × 4 × 1 Γ-centered *k*-meshes for FM configurations in *C*2/*m* and *R*-3*m* phases makes the grid spacing of *k*-meshes reaching $2\pi \times 0.04$ $Å^{-1}$ or less. Meanwhile, adaptive *k*-points were used for supercells in different AFM configurations that are shown in figure 2. We take $Cs_4CuSb_2Cl_{12}$ as an example. For AFM configurations of *C*2/*m* phase, 4 × 4 × 1 Γ-centered *k*-mesh is used for AFM-1 ($a = b = 7.734$ Å, $c = 26.889$ Å) and 2 × 2 × 2 Γ-centered *k*-mesh is used for AFM-2 ($a = 13.510$ Å, $b = 14.891$ Å, $c = 13.475$ Å) and AFM-3 ($a = 13.510$ Å, $b = 14.891$ Å, $c = 13.475$ Å). For AFM configurations of *R*-3*m* phase, 2 × 4 × 1 Γ-centered *k*-mesh is employed for AFM-1 ($a = 15.395$ Å, $b = 7.713$ Å, $c = 37.285$ Å). The grid spacing of k-mesh for AFM configurations is $2\pi \times 0.05$ $Å^{-1}$ or less. We performed test calculations of convergence using denser *k*-point meshes for FM configurations and supercells in AFM configurations, and found the change of calculated total energies are less than 1 meV/atom. It means currently used *k*-mesh is enough to give reseaonable description of properties.

Ab initio molecular dynamics simulations (AIMD) were performed in the VASP code to verify the themal stability of $Cs_4ScSb_2Br_{12}$. The calculation were carried out using a 2 × 2 × 2 supercell (152 atoms) of the primitive cell in *C*2/*m* symmetry and using 2 × 2 × 1 Γ-centered k-mesh in the first Brillouin zone. A Nosé–Hoover thermostat was applied to simulate a canonical ensemble at the temperature of 300 K [31]. A total simulation time of 3 ps and time step of 1 fs was used.

3. Crystal structure

⟨1 1 1⟩ layered double perovskite $Cs_4MSb_2X_{12}$ in *C*2/*m* or *R*-3*m* phase can be regarded as one MX_6 octahedral layers being inserted into the $[Sb_2X_9]$ bilayers of parent $Cs_3Sb_2X_9$ [12]. Thus, ⟨1 1 1⟩ layered double perovskite has higher electronic dimensionality than parent $Cs_3Sb_2X_9$. Meanwhile ⟨1 1 1⟩ layered double perovskite can also be treated as M or Sb-deficient derivatives compared to the three-dimensional double perovskite [32]. The emergence of layered double perovskite $Cs_4MSb_2X_{12}$ provides a huge space for searching candidates as photovoltaic and spintronic materials.

4. Results and discussion

4.1. Thermodynamic stability

We combined high-throughput calculations with Materials Project (a material database) [33] to accelerate the evaluation

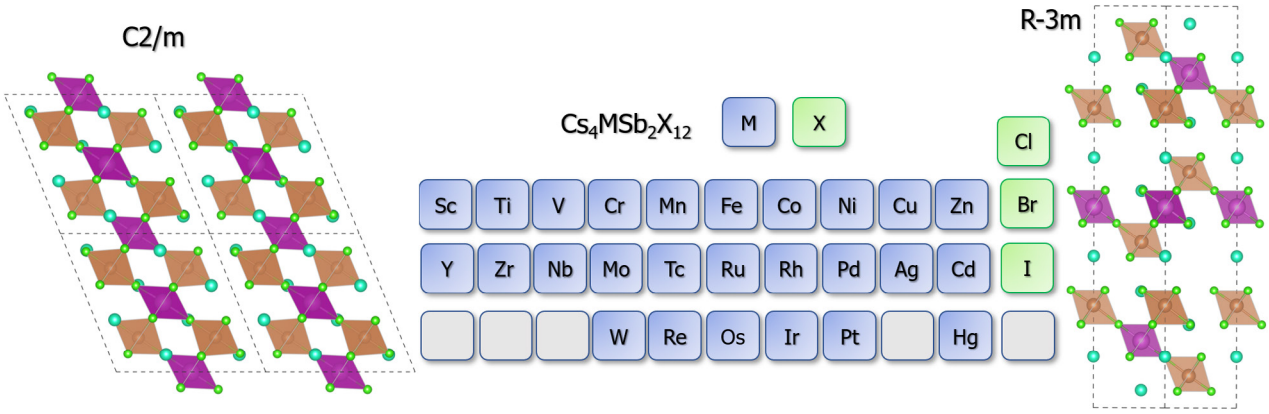

Figure 1. Crystal structures of $Cs_4MSb_2X_{12}$ (M: +2 transition metals; X: Cl, Br and I) in *C*2/*m* and *R*-3*m* phase. *C*2/*m* and *R*-3*m* phases are experimental structures of $Cs_4CuSb_2Cl_{12}$ and $Cs_4MnSb_2Cl_{12}$, respectively. Left panel and right panel are crystal structures of *C*2/*m* phase and *R*-3*m* phase. Balls in green and cyan represent halogens and Cs atoms, respectively. Brown octahedron and purple octahedron denote SbX_6 and MX_6, respectively. The middle panel shows substitutional elements we considered. The elements in blue squares are transition metals have +2 charged state while those in green squares are halogens.

Table 1. Energy above hull (meV/atom) and magnetic moments (μ_B) of six thermodynamically stable compounds in *C*2/*m* and *R*-3*m* phases with FM ordering.

	Energy above hull (meV/atom)		Magnetic moment (μ_B)	
Compound	*C*2/*m*	*R*-3*m*	*C*2/*m*	*R*-3*m*
$Cs_4MnSb_2Cl_{12}$	−0.30	−0.32	5.00	5.00
$Cs_4CuSb_2Cl_{12}$	−3.40	4.64	1.00	0.00
$Cs_4ScSb_2Br_{12}$	−14.20	88.03	1.00	0.86
$Cs_4CdSb_2Cl_{12}$	−1.00	−0.51	0	0
$Cs_4AgSb_2Br_{12}$	−6.60	−5.11	0	0
$Cs_4AgSb_2Cl_{12}$	−8.40	−5.98	0	0

of thermodynamic stability of $Cs_4MSb_2X_{12}$. The energy above hull, i.e. the energy difference between targeted compound and phase-separated combinations of compounds with the lowest energy at the associated composition, were calculated by retrieving the total energies of all available compounds in the Cs–M–Sb–X system including binaries and ternaries from Materials Project. If the energy above hull value is negative, the compound $Cs_4MSb_2X_{12}$ is thermodynamically stable, meaning it could be experimentally synthesized. Based on it, six thermodynamically stable candidates are screened out among 78 $Cs_4MSb_2X_{12}$ (M: +2 transition metals; X: Cl, Br and I). They are $Cs_4MnSb_2Cl_{12}$, $Cs_4CuSb_2Cl_{12}$, $Cs_4ScSb_2Br_{12}$, $Cs_4CdSb_2Cl_{12}$, $Cs_4AgSb_2Br_{12}$ and $Cs_4AgSb_2Cl_{12}$. Their energies above hull values and the magnetic moments are summarized in table 1.

Among these six candidates in FM ordering, $Cs_4MnSb_2Cl_{12}$, $Cs_4CuSb_2Cl_{12}$ and $Cs_4ScSb_2Br_{12}$ shows magnetism while $Cs_4CdSb_2Cl_{12}$, $Cs_4AgSb_2Br_{12}$ and $Cs_4AgSb_2Cl_{12}$ do not show magnetism, which means the former have the potential to be spintronic materials while the latter do not. Thus, we do not discuss properties of $Cs_4CdSb_2Cl_{12}$, $Cs_4AgSb_2Br_{12}$ and $Cs_4AgSb_2Cl_{12}$ in this paper considering our intention. Our calculation shows $Cs_4MnSb_2Cl_{12}$ and $Cs_4CuSb_2Cl_{12}$ are thermodynamically stable, which is in accordance with the reported result that $Cs_4MnSb_2Cl_{12}$ and $Cs_4CuSb_2Cl_{12}$ were successfully synthesized. It means our high-throughput calculation is valid for screening the thermodynamically stable ⟨1 1 1⟩ layered magnetic double perovskites. Meanwhile, $Cs_4ScSb_2Br_{12}$ is predicted for the first time. The thermal stability of $Cs_4ScSb_2Cl_{12}$ is futher verified by AIMD simulation. Compared the initial structure at 0 K with snapshot of $Cs_4ScSb_2Br_{12}$ after ~3 ps simulations collected at targeted temperature 300 K, the $Cs_4ScSb_2Cl_{12}$ only went through slight distortion as shown in figure S1 (stacks.iop.org/JPhysCM/32/225705/mmedia), verifying its thermal stability at room temperature.

4.2. Magnetic ground states

To identify the magnetic ground state configuration of three thermodynamically stable magnetic compounds ($Cs_4MnSb_2Cl_{12}$, $Cs_4CuSb_2Cl_{12}$, $Cs_4ScSb_2Br_{12}$), we constructed three supercells with AFM ordering of the on-site spin using *C*2/*m* phase and one supercell with AFM ordering of the on-site spin using *R*-3*m* phase, which are shown in figure 2. Then, the energy differences between configurations with FM and AFM ordering are tabulated in table 2 to compare the relative stability.

We found that all three compounds favor the AFM configuration as the magnetic ground state. For $Cs_4MnSb_2Cl_{12}$ in *C*2/*m* phase, the AFM-3 has the lowest total energy, which is 2.0 meV lower than that of FM configuration. While for $Cs_4MnSb_2Cl_{12}$ in *R*-3*m* phase, AFM-1 configuration is more stable, which is 736.3 meV lower than that of FM configuration. Comparing the total energy of $Cs_4MnSb_2Cl_{12}$ in *C*2/*m* phase with AFM-3 configuration and that in *R*-3*m* phase with AFM-1 configuration, the latter has lower total energy. Thus, *R*-3*m* symmetry with AFM configuration should be the ground state structure of $Cs_4MnSb_2Cl_{12}$, which is consistent with experimental observations [15]. Slightly different from the case of $Cs_4MnSb_2Cl_{12}$, $Cs_4CuSb_2Cl_{12}$ and $Cs_4ScSb_2Br_{12}$ favor *C*2/*m* phase as ground state structure. For $Cs_4CuSb_2Cl_{12}$ in *C*2/*m* phase, AFM-3

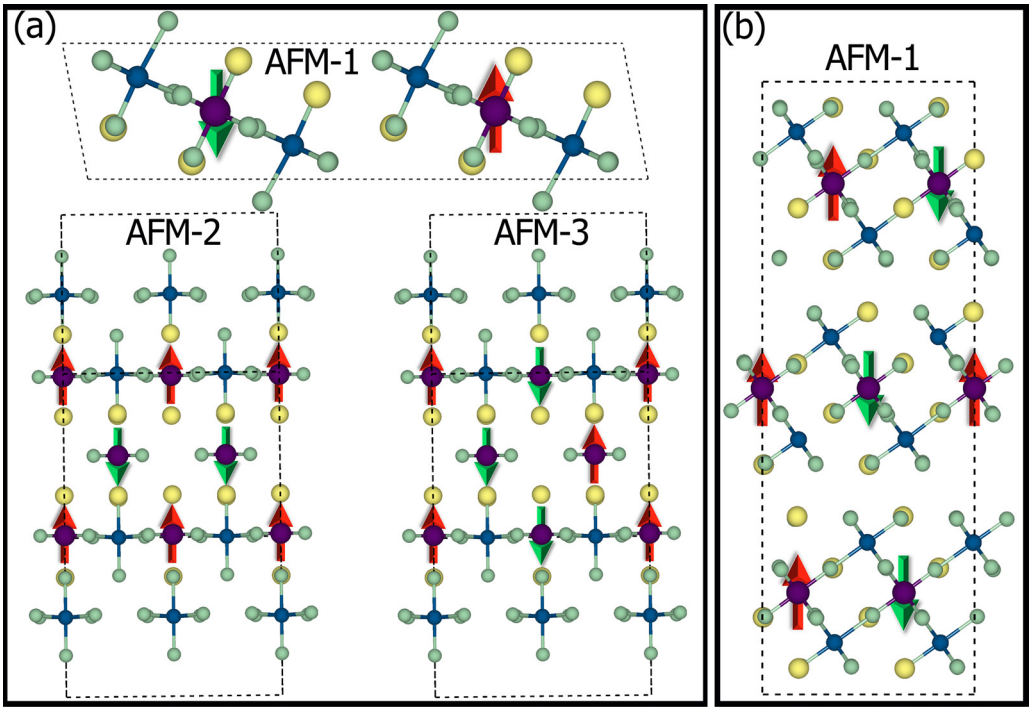

Figure 2. Schematic diagrams of supercells with AFM orderings: (a) three AFM configurations in *C*2/*m* phase and (b) one AFM configuration in *R*-3*m*. Red arrow denotes spin-up magnetic metals meanwhile blue arrow denotes spin-down magnetic metals.

Table 2. Relative total energy meV/formula (19 atoms in one formula, i.e. one magnetic atom in one formula) of $Cs_4MnSb_2Cl_{12}$, $Cs_4CuSb_2Cl_{12}$, and $Cs_4ScSb_2Br_{12}$ in different magnetic ordering. GGA + *U* is used for the total energy calculation of $Cs_4MnSb_2Cl_{12}$ ($U_{eff} = 2.0$) [27, 28] and $Cs_4CuSb_2Cl_{12}$ ($U_{eff} = 8.5$) [29, 30] while GGA (PBE) is used for $Cs_4ScSb_2Br_{12}$. The configuration with lowest total energy is taken as reference.

	$Cs_4MnSb_2Cl_{12}$		$Cs_4CuSb_2Cl_{12}$		$Cs_4ScSb_2Br_{12}$	
Compound	*C*2/*m*	*R*-3*m*	*C*2/*m*	*R*-3*m*	*C*2/*m*	*R*-3*m*
FM	737.5	736.3	8.1	456.1	19.3	6.6
AFM-1	736.8	0	7.5	50.5	1.1	5.0
AFM-2	967.2	/	76.9	/	0.0	/
AFM-3	735.5	/	0	/	0.7	/

configuration has the lowest total energy, being the magnetic ground states, which is in line with previous experimental and theoretical results [13, 34]. For $Cs_4ScSb_2Br_{12}$ in *C*2/*m* phase, the total energy of AFM-2 configuration is the lowest, denoting it is the magnetic ground states.

4.3. Electronic and magnetic properties

To discuss the electronic properties of $Cs_4MnSb_2Cl_{12}$, $Cs_4CuSb_2Cl_{12}$ and $Cs_4ScSb_2Br_{12}$, we calculated the orbital-projected density of states (DOS) of supercell in the magnetic ground states, as depicted in figure 3. The magnetic ground states of $Cs_4MnSb_2Cl_{12}$ (*R*-3*m* symmetry with AFM-1 ordering) and $Cs_4CuSb_2Cl_{12}$ (*C*2/*m* symmetry with AFM-3 ordering) are semiconductors. The GGA + U band gap of $Cs_4MnSb_2Cl_{12}$ is 1.75 eV, which is lower than experimental reported band gap 2.98 eV [15]. The VBM of $Cs_4MnSb_2Cl_{12}$ is composed of Mn-3d, Sb-5s and Cl-3p orbitals, and CBM is composed of Mn-3d, Sb-5p and Cl-3p orbitals. Both VBM and CBM of $Cs_4MnSb_2Cl_{12}$ have strong p-d hybridization. The GGA + U band gap of $Cs_4CuSb_2Cl_{12}$ is 0.93 eV, which is slightly lower than the experimental reported value 1.03 eV [13]. The VBM of $Cs_4CuSb_2Cl_{12}$ is composed of Sb-5s and Cl-3p orbitals, and its CBM is composed of Cu-3d and Cl-3p orbitals.

Different from the cases of $Cs_4MnSb_2Cl_{12}$ and $Cs_4CuSb_2Cl_{12}$, the magnetic ground state of $Cs_4ScSb_2Br_{12}$ in *C*2/*m* phase with AFM-2 ordering shows metallicity. We use GGA + *U* ($U_{eff} = 2.5$ eV) [35] and hybrid functional (HSE06) [36] to verify whether the metallicity of $Cs_4ScSb_2Br_{12}$ in magnetic ground state is due to the general underestimation of the band gap caused by PBE functional or not. The metallicity of $Cs_4ScSb_2Br_{12}$ in *C*2/*m* phase is still preserved even using GGA + *U* and HSE06 functional.

From DOS, we can see there is a strong coupling between M-d and X-p orbitals in $Cs_4MnSb_2Cl_{12}$ and $Cs_4ScSb_2Br_{12}$. Since the distance between two first nearest-neighboring (NN) M ions is quite large (>7 Å), the direct exchange coupling between two NN M ions is exceptionally weak [37–39]. But the NN M-d ions could interact with each other through the bridging BX_6 octahedron via the supersuperexchange mechanism [40, 41], which could be facilitated by the strong

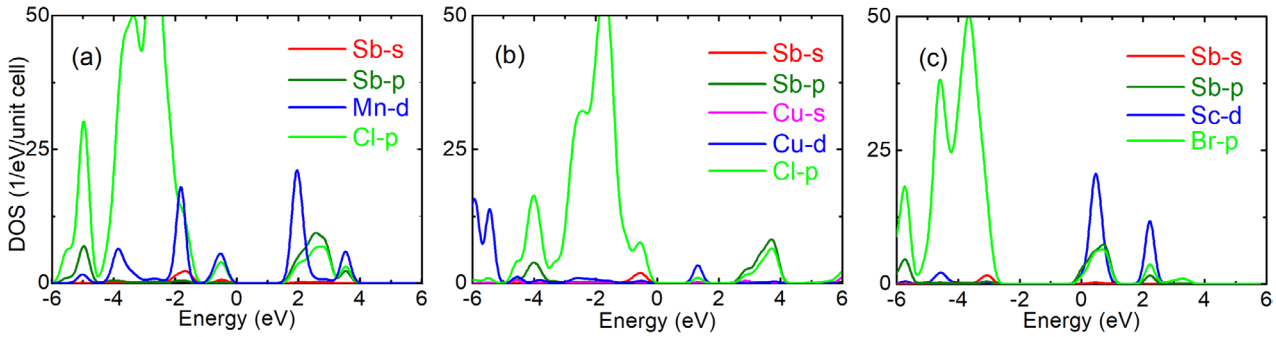

Figure 3. DOS of ground magnetic states of (a) $Cs_4MnSb_2Cl_{12}$, (b) $Cs_4CuSb_2Cl_{12}$ and (c) $Cs_4ScSb_2Br_{12}$.

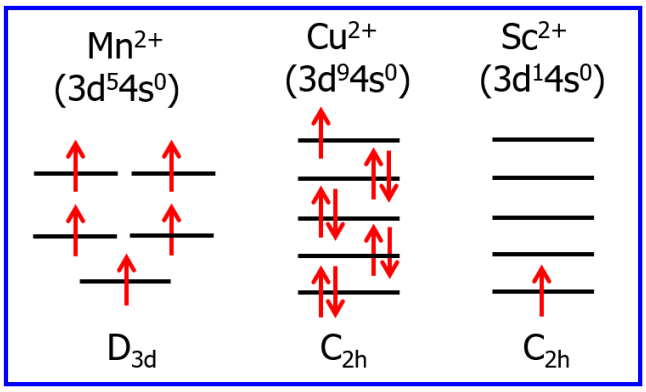

Figure 4. Schematic diagram of electron occupation of Mn^{2+}, Cu^{2+} and Sc^{2+} in $Cs_4MnSb_2Cl_{12}$, $Cs_4CuSb_2Cl_{12}$ and $Cs_4ScSb_2Br_{12}$, respectively.

coupling between M-d and X-p orbitals. In addition, local magnetic moments in $Cs_4MnSb_2Cl_{12}$ ($\mu_B = 5$), $Cs_4CuSb_2Cl_{12}$ ($\mu_B = 1$) and $Cs_4ScSb_2Br_{12}$ ($\mu_B = 1$) are contributed by M-d orbitals. Mn^{2+} ions in $Cs_4MnSb_2Cl_{12}$ favor high spin configuration ($d^5\uparrow d^0\downarrow$). And based on crystal field theory, five d orbitals of Mn^{2+} will split into singlet A_1g (d_{z2}), doublet Eg ($d_{xz} + d_{yz}$) and doublet Eg′ ($d_{xy} + d_{x2} - d_{y2}$) under a D_{3d} symmetry [42], as shown in figure 4. The d orbitals of Cu^{2+} ($d^5\uparrow d^4\downarrow$) and Sc^{2+} ($d^1\uparrow d^0\downarrow$) in $Cs_4CuSb_2Cl_{12}$ and $Cs_4ScSb_2Br_{12}$ will show five crystal field states under the symmetry of C_{2h} symmetry [42], as depicted in figure 4.

For spintronic application, the magnetic ordering temperature is important. The Néel temperature of $Cs_4MnSb_2Cl_{12}$ (AFM ground-state) is calculated to be ~1 K [40], showing the potential of layered double perovskite as spintronics. But for $Cs_4CuSb_2Cl_{12}$ and $Cs_4ScSb_2Br_{12}$, Néel temperature is not discussed in this work. It would be calculated in future study.

5. Conclusion

We investigated a series of ⟨1 1 1⟩-oriented layered double perovskites $Cs_4MSb_2X_{12}$ (M: +2 transition metals, X: Cl, Br and I), and identified three thermodynamically stable layered double perovskites $Cs_4MnSb_2Cl_{12}$, $Cs_4CuSb_2Cl_{12}$ and $Cs_4ScSb_2Br_{12}$ by high-throughput first-principles calculations. The ground state structure of $Cs_4MnSb_2Cl_{12}$ has the *R*-3*m* symmetry and exhibits AFM ordering, while the $Cs_4CuSb_2Cl_{12}$ and $Cs_4ScSb_2Br_{12}$ favor the *C*2/*m* symmetry and show AFM ordering. In spite of that we did not find thermodynamically stable $Cs_4MSb_2X_{12}$ showing FM ordering, our high-throughput calculation is valid for searching the thermodynamically stable ⟨1 1 1⟩ layered magnetic double perovskites considering that the calculated results are consistent with the experimental observations. Additionally, a new layered double perovskite $Cs_4ScSb_2Br_{12}$ is predicted for the first time and it may be synthesized experimentally in the future. Our first-principles calculations show that $Cs_4MnSb_2Cl_{12}$, $Cs_4CuSb_2Cl_{12}$ and $Cs_4ScSb_2Br_{12}$ with AFM ordering can be spintronic materials, which validates the extension of layered double materials from photovoltaics to spintronics.

Acknowledgments

This work was supported by National Natural Science Foundation of China (NSFC) under Grant Nos. 61722402, 61574059 and 91833302, National Key Research and Development Program of China (2016YFB0700700), Shanghai Academic/Technology Research Leader (19XD1421300), Fok Ying Tung Education Foundation (161060), the Fundamental Research Funds for the Central Universities and CC of ECNU. We thank Dr Wei Luo and Dr Ke Xu for helpful discussions.

ORCID iDs

Shiyou Chen https://orcid.org/0000-0002-4039-8549

References

[1] Zhao X G, Yang J H, Fu Y, Yang D, Xu Q, Yu L, Wei S H and Zhang L 2017 Design of lead-free inorganic halide perovskites for solar cells via cation-transmutation *J. Am. Chem. Soc.* **139** 2630

[2] Volonakis G, Haghighirad A A, Milot R L, Sio W H, Filip M R, Wenger B, Johnston M B, Herz L M, Snaith H J and Giustino F 2017 $Cs_2InAgCl_6$: a new lead-free halide double perovskite with direct band gap *J. Phys. Chem. Lett.* **8** 772

[3] Volonakis G, Filip M R, Haghighirad A A, Sakai N, Wenger B, Snaith H J and Giustino F 2016 Lead-free halide double perovskites via heterovalent substitution of noble metals *J. Phys. Chem. Lett.* **7** 1254

[4] Mcclure E T, Ball M R, Windl W and Woodward P M 2016 Cs_2AgBiX_6 (X = Br, CI): New visible light absorbing,

lead-free halide perovskite semiconductors *Chem. Mater.* **28** 1348
[5] Slavney A H, Hu T, Lindenberg A M and Karunadasa H I 2016 A bismuth-halide double perovskite with long carrier recombination lifetime for photovoltaic applications *J. Am. Chem. Soc.* **138** 2138
[6] Wei F, Deng Z, Sun S, Xie F, Kieslich G, Evans D M, Carpenter M A, Bristowe P D and Cheetham A K 2016 The synthesis, structure and electronic properties of a lead-free hybrid inorganic–organic double perovskite $(MA)_2KBiCl_6$ (MA = Methylammonium) *Mater. Horiz.* **3** 328
[7] Filip M R, Hillman S, Haghighirad A A, Snaith H J and Giustino F 2016 Band gaps of the lead-free halide double perovskites $Cs_2BiAgCl_6$ and $Cs_2BiAgBr_6$ from theory and experiment *J. Phys. Chem. Lett.* **7** 2579
[8] Igbari F, Wang Z K and Liao L S 2019 Progress of lead-free halide double perovskites *Adv. Energy Mater.* **9** 1803150
[9] Savory C N, Walsh A and Scanlon D O 2016 Can Pb-free halide double perovskites support high-effciency solar cells? *ACS Energy Lett.* **1** 949
[10] Cai B, Chen X, Xie M, Zhang S, Liu X, Yang J, Zhou W, Guo S and Zeng H 2018 A class of Pb-free double perovskite halide semiconductors with intrinsic ferromagnetism, large spin splitting and high Curie temperature *Mater. Horiz.* **5** 961
[11] Wang X-D, Miao N-H, Liao J-F, Li W-Q, Xie Y, Chen J, Sun Z-M, Chen H-Y and Kuang D-B 2019 The top-down synthesis of single-layered $Cs_4CuSb_2Cl_{12}$ halide perovskite nanocrystals for photoelectrochemical application *Nanoscale* **11** 5180
[12] Tang G, Xiao Z, Hosono H, Kamiya T, Fang D and Hong J 2018 Layered halide double perovskites $Cs_{3+n}M(II)_nSb_2X_{9+3n}$ (M = Sn, Ge) for photovoltaic applications *J. Phys. Chem. Lett.* **9** 43
[13] Vargas B, Ramos E, Perez-Gutierrez E, Alonso J C and Solis-Ibarra D 2017 A direct bandgap copper-antimony halide perovskite *J. Am. Chem. Soc.* **139** 9116
[14] Xu J, Liu J-B, Wang J, Liu B-X and Huang B 2018 Prediction of novel p-type transparent conductors in layered double perovskites: a first-principles study *Adv. Funct. Mater.* **28** 1800332
[15] Vargas B *et al* 2018 Optical, electronic, and magnetic engineering of ⟨1 1 1⟩ layered halide perovskites *Chem. Mater.* **30** 5315
[16] Singhal N, Chakraborty R, Ghosh P and Nag A 2018 Low-bandgap $Cs_4CuSb_2Cl_{12}$ layered double perovskite: synthesis, reversible thermal changes, and magnetic interaction *Chem. Asian J.* **13** 2085
[17] Gong C, Li L, Li Z, Ji H, Stern A, Xia Y, Cao T, Bao W, Wang C and Wang Y 2017 Discovery of intrinsic ferromagnetism in two-dimensional van der Waals crystals *Nature* **546** 265
[18] Huang B, Clark G, Navarro-Moratalla E, Klein D R, Cheng R, Seyler K L, Zhong D, Schmidgall E, Mcguire M A and Cobden D H 2017 Layer-dependent ferromagnetism in a van der Waals crystal down to the monolayer limit *Nature* **546** 270
[19] Li X and Yang J 2014 $CrXTe_3$ (X = Si, Ge) nanosheets: two dimensional intrinsic ferromagnetic semiconductors *J. Mater. Chem.* C **2** 7071
[20] Kan E, Li M, Hu S, Xiao C, Xiang H and Deng K 2013 Two-dimensional hexagonal transition-metal oxide for spintronics *J. Phys. Chem. Lett.* **4** 1120
[21] Zhou P, Sun C Q and Sun L Z 2016 Two dimensional antiferromagnetic chern insulator: $NiRuCl_6$ *Nano Lett.* **16** 6325
[22] Perdew J P, Burke K and Ernzerhof M 1996 Generalized gradient approximation made simple *Phys. Rev. Lett.* **77** 3865
[23] Kresse G and Furthmuller J 1996 Efficient iterative schemes for *ab initio* total-energy calculations using a plane-wave basis set *Phys. Rev.* B **54** 11169
[24] Kresse G and Furthmuller J 1996 Efficiency of ab-initio total energy calculations for metals and semiconductors using a plane-wave basis set *Comput. Mater. Sci.* **6** 15
[25] Rappe A M, Rabe K M, Kaxiras E and Joannopoulos J D 1990 Optimized pseudopotentials *Phys. Rev.* B **41** 1227
[26] Dudarev S, Botton G, Savrasov S, Humphreys C and Sutton A 1998 Electron-energy-loss spectra and the structural stability of nickel oxide: an LSDA + *U* study *Phys. Rev.* B **57** 1505
[27] Zhang J, Lu X, Zhou J, Su J, Min K, Huang F and Zhu J 2010 First-principles study of structural, electronic, and magnetic properties of double perovskite Ho_2MnFeO_6 *Phys. Rev.* B **82** 224413
[28] Xiang H, Wei S-H, Whangbo M-H and Da Silva J L 2008 Spin-orbit coupling and ion displacements in multiferroic $TbMnO_3$ *Phys. Rev. Lett.* **101** 037209
[29] Heinemann M, Eifert B and Heiliger C 2013 Band structure and phase stability of the copper oxides Cu_2O, CuO, and Cu_4O_3 *Phys. Rev.* B **87** 115111
[30] Himmetoglu B, Wentzcovitch R M and Cococcioni M 2011 First-principles study of electronic and structural properties of CuO *Phys. Rev.* B **84** 115108
[31] Shuichi N 1984 A unified formulation of the constant temperature molecular dynamics methods *J. Chem. Phys.* **81** 511
[32] Saparov B, Hong F, Sun J P, Duan H S, Meng W, Cameron S, Hill I G, Yan Y and Mitzi D B 2015 Thin-film preparation and characterization of $Cs_3Sb_2I_9$: a lead-free layered perovskite semiconductor *Chem. Mater.* **27** 5622
[33] Jain A *et al* 2013 Commentary: The materials project: a materials genome approach to accelerating materials innovation *APL Mater.* **1** 011002011002
[34] Wang X, Meng W, Xiao Z, Wang J, Mitzi D and Yan Y 2017 First-principles understanding of the electronic band structure of copper-antimony halide perovskite: the effect of magnetic ordering (arXiv:1707.09539) (unpublished)
[35] He J and Franchini C 2012 Screened hybrid functional applied to $3d^0 \rightarrow 3d^8$ transition-metal perovskites $LaMO_3$ (M = Sc–Cu): Influence of the exchange mixing parameter on the structural, electronic, and magnetic properties *Phys. Rev.* B **86** 235117
[36] Heyd J, Scuseria G E and Ernzerhof M 2003 Hybrid functionals based on a screened coulomb potential *J. Chem. Phys.* **118** 8207
[37] Kanamori J 1959 Superexchange interaction and symmetry properties of electron orbitals *J. Phys. Chem. Solids* **10** 87
[38] Goodenough J B 1955 Theory of the role of covalence in the perovskite-type manganites [La, M(II)]MnO_3 *Phys. Rev.* **100** 564
[39] Anderson P 1950 Antiferromagnetism. Theory of superexchange interaction *Phys. Rev.* **79** 350
[40] Xu J, Xu C, Liu J-B, Bellaiche L, Xiang H, Liu B-X and Huang B 2019 Prediction of room-temperature half-metallicity in layered halide double perovskites *npj Comput. Mater.* **5** 1
[41] Marjerrison C, Thompson C, Sharma A, Hallas A, Wilson M, Munsie T, Flacau R, Wiebe C, Gaulin B and Luke G 2016 Magnetic ground states in the three Os^{6+} ($5d^2$) double perovskites Ba_2MOsO_6 (M = Mg, Zn, and Cd) from Néel order to its suppression *Phys. Rev.* B **94** 134429
[42] Burns R G and Burns R G 1993 *Mineralogical Applications of Crystal Field Theory* vol 5 (Cambridge: Cambridge University Press)